The Functionality of the three-sited Ferroxidase center of E. coli Bacterial Ferritin (EcFtnA)

The Functionality of the Three-Sited Ferroxidase Center of E. coli Bacterial Ferritin (EcFtnA)

Journal:	*Biochemistry*
Manuscript ID:	bi-2013-01517f
Manuscript Type:	Article
Date Submitted by the Author:	10-Nov-2013
Complete List of Authors:	Bou-Abdallah, Fadi; State University of New York, Chemistry Yang, Huidong; SUNY Potsdam, Chemistry Awomolo, Adeola; SUNY Potsdam, Chemistry Cooper, Brenna; SUNY Potsdam, Chemistry Woodhall, Mark; University of Reading, Microbial Biochemistry Andrews, Simon; University of Reading, Microbial Biochemistry Chasteen, N Dennis; University of New Hampshire, Chemistry

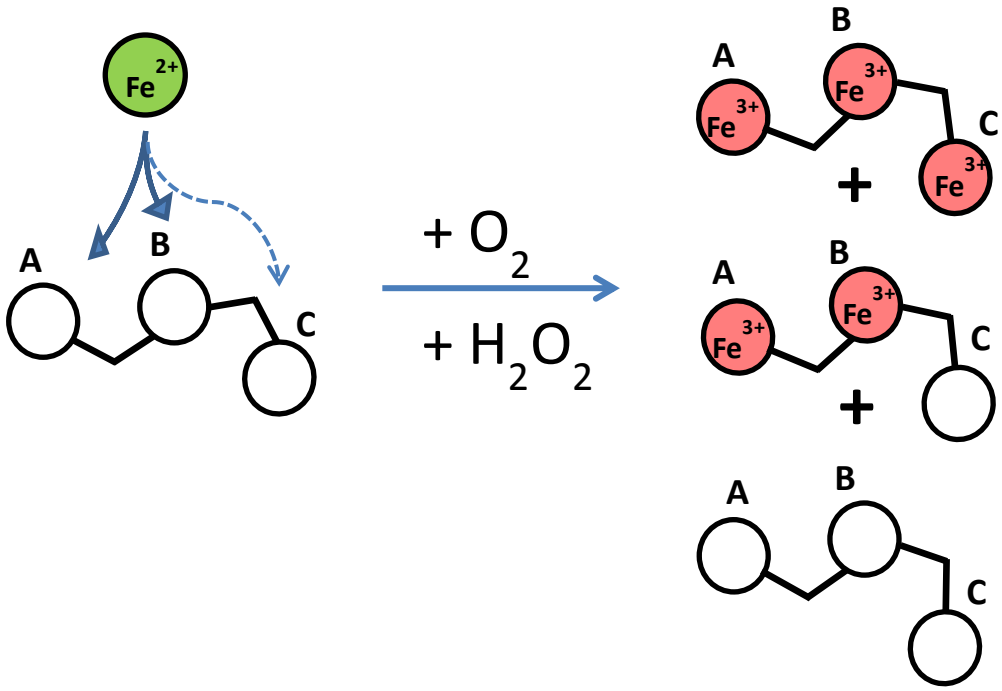
Fe 2+
A
B
C
+ O2
+ H2O2
B
A
Fe 3+
Fe 3+
C
Fe 3+
+
B
A
Fe 3+
Fe 3+
C
+
A
B
C

The Functionality of the Three-Sited Ferroxidase Center of *E. coli* Bacterial Ferritin (EcFtnA) [*]

F. Bou-Abdallah[#, §], H. Yang[#], A. Awomolo[#], B. Cooper[#], M. R. Woodhall[¶], S. C. Andrews[¶], and N. D. Chasteen[‡]

[#] Department of Chemistry, State University of New York, Potsdam, NY 13676, USA, [¶] Microbial Biochemistry, School of Animal & Microbial Sciences, University of Reading, Whiteknights, PO Box 228, Reading RG6 6AJ, UK and [‡] Department of Chemistry, University of New Hampshire, Durham, NH 03824, USA.

[#] This work was supported by a Cottrell College Science Award (ID # 7892) from Research Corporation (F.B.A.), grant R01 GM20194 from the National Institute of General Medical Sciences (N.D.C.), and by the Reading Endowment Trust Fund (S.C.A.)

Keywords: kinetics, bacterial ferritin (EcFtnA), EPR, iron oxidation, site-directed mutagenesis**,** C-site, trinuclear ferroxidase center, H_2O_2

[§] To whom correspondence should be addressed: Dept. of Chemistry, Stowell Hall, State University of New York at Potsdam, Potsdam, NY 13676. Tel.: 315-267-2268; Fax: 315-267-3170; E-mail: bouabdf@potsdam.edu

ABSTRACT

At least three ferritins are found in the bacterium *Escherichia coli*, the heme-containing bacterioferritin (EcBFR) and two non-heme bacterial ferritins (EcFtnA and EcFtnB). In addition to the conserved A- and B-sites of the diiron ferroxidase center, EcFtnA has a third iron-binding site (the C-site) of unknown function that is nearby the diiron site. In the present work, the complex chemistry of iron oxidation and deposition in EcFtnA has been further defined through a combination of oximetry, pH stat, stopped-flow and conventional kinetics, UV-visible, fluorescence and EPR spectroscopic measurements on the wild-type protein and site-directed variants of the A-, B- and C-sites. The data reveal that, while H_2O_2 is a product of dioxygen reduction in EcFtnA and oxidation occurs with a stoichiometry of Fe(II)/O_2 ~ 3:1, most of the H_2O_2 produced is consumed in subsequent reactions with a 2:1 Fe(II)/H_2O_2 stoichiometry, thus suppressing hydroxyl radical formation. While the A- and B-sites are essential for rapid iron oxidation, the C-site slows oxidation and suppresses iron turnover at the ferroxidase center. A tyrosyl radical, assigned to Tyr24 near the ferroxidase center, is formed during iron oxidation and its possible significance to the function of the protein is discussed. Taken as a whole, the data indicate that there are multiple iron-oxidation pathways in EcFtnA with O_2 and H_2O_2 as oxidants. Furthermore, the data are inconsistent with the C-site being a transit site, providing iron to the A- and B-sites, and does not support a universal mechanism for iron oxidation in all ferritins as recently proposed.

Abbreviations: AfFtn, *Archaeoglobus fulgidus* ferritin; AvBF, *Azotobacter vinelandii* ferritin; PfFtn, *Pyrococcus furiosus* ferritin; DvFtn, *Desulfovibrio vulgaris* Hildenborough ferritin Dps; EcBFR, *Escherichia coli* heme-containing bacterioferritin; EcFtnA, *Escherichia coli* non-heme bacterial ferritin type A; EcFtnB, *Escherichia coli* non-heme bacterial ferritin type B; HpF, *Helicobacter pylori* ferritin; LiDps, *Listeria innocua* Dps ferritin; HuHF, human H-chain ferritin; HuLF, human L-chain ferritin; HoSF, horse spleen ferritin; **D**NA binding **p**roteins from **s**tarved cells; EMPO, 5-ethoxycarbonyl-5-methyl-1-pyrroline-N-oxide; EPR, electron paramagnetic resonance; ITC, isothermal titration calorimetry; Mes, 2-(N-morpholino) ethanesulfonic acid; Mops, 3-(N-morpholino) propanesulfonic acid.

INTRODUCTION

Iron is an essential element for life in large part due to its ability to accept and donate electrons readily in cellular redox processes. However, iron can also present a danger to the cell by catalyzing the conversion of superoxide and hydrogen peroxide to free radical species that damage cellular membranes, lipids, proteins, and DNA (*1*). In oxygenated environments, both prokaryotes and eukaryotes have developed highly efficient mechanisms to acquire iron and ensure its bioavailability while preventing toxicity (*1*). Ferritin, a widely distributed intracellular iron storage and detoxification protein, consists of two functionally and genetically distinct H and L subunit types in mammals. These two subunits co-assemble in various ratios to form a shell-like structure where thousands of iron atoms can be stored within the central 8 nm diameter cavity. The H-subunit has a dinuclear iron center consisting of A and B binding sites where the fast conversion of Fe^{2+} to Fe^{3+} by dioxygen occurs (*1-5*). Recently a third Fe^{3+} site, a C-site involving Glu140, has been identified in HuHF and proposed to function as a transit site feeding iron to the ferroxidase center (*6-8*). This site is different from the earlier postulated nucleation site in HuHF involving Glu64 and Glu67 which has since been shown not to be essential for core mineralization (*5*). In heteropolymeric mammalian ferritins, the L-subunit lacks a ferroxidase center and has a greater density of acidic groups on the inner surface of the cavity, and so is thought to contribute to the nucleation of the iron core (*2-4,9*).

The bacterium *Escherichia coli* produces at least two true ferritins which exhibit fast iron ferroxidation reactions: a heme-containing 'bacterioferitin' (EcBFR) and a non-heme ferritin (EcFtnA). A third non-heme ferritin-type protein (EcFtnB) lacks this fast iron oxidizing property and it is unclear whether this protein has an iron-storage function (*1,9*). EcFtnA, the subject of this work, is a homopolymer of 24 identical subunits and has a well established C-site that is positioned ~ 11 Å from the A-site and ~ 7 Å from the B-site of the ferroxidase center (Fig. 1) (*10*). Isothermal titration calorimetry

(ITC) measurements of Fe^{2+} binding to EcFtnA (*11)* indicated the presence of two classes of strong binding site each with a binding stoichiometry of ~ 24 Fe(II) per protein shell at pH 7.0, corresponding to the binding of 2 Fe^{2+} to the A- and B-sites of each of the 24 dinuclear ferroxidase centers. Additional uncharacterized weak binding was also observed and presumably involves binding at the C-site among other possibilities. The ITC data revealed that the C-site, the proposed transit site (*6-8*), is not involved in strong Fe^{2+} binding but modulates Fe^{2+} binding at the adjacent dinuclear A and B iron sites. In addition, the ITC data suggested the presence of inter- and intra-subunit negative cooperativity between the A-, B- and C-binding sites within the ferroxidase center and between ferroxidase centers located on separate subunits within the protein shell (*11*).

Numerous studies have been directed at elucidating the detailed mechanism of iron oxidation in ferritins (*1-53*). While a μ-peroxo diiron(III) intermediate is observed in some, it is not observed in all ferritins despite the similarities in their amino acid sequences, structures and ferroxidase center residues. For example, the blue peroxo intermediate (λ_{max} ~ 650 nm) has not been observed in EcBFR and the H-chain from recombinant frog ferritin (*20,23*) whereas in HuHF, horse spleen ferritin (HoSF), M-chain from recombinant frog ferritin, EcFtnA, and human mitochondrial ferritin (MtF), the blue complex is readily detected by stopped-flow spectrophotometry (*13-19*). In addition, the H_2O_2 that is produced during iron oxidation at the dinuclear ferroxidase centers is used differently by these ferritins; EcBFR quickly consumes one H_2O_2 to oxidize two Fe^{2+} at a second diiron site (*20*) whereas in other ferritins it accumulates to measurable amounts in solution (*12-18,28*). Furthermore, in HuHF two Fe^{2+} ions are oxidized by one H_2O_2, thus avoiding the generation of hydroxyl radicals whereas MtF lacks this Fe^{2+} + H_2O_2 detoxification property and, unlike other ferritins, utilizes only 12 of its 24 ferroxidase centers (*18,24*). These mechanistic differences point towards the importance of second shell amino acids in

modulating the chemistry of iron oxidation at the dinuclear ferroxidase center of ferritins and argue against the recently proposed common mechanism for all ferritins (*8*).

In ferritins where Fe^{2+} oxidation by O_2 produces a peroxo complex, the intermediate quickly decays to the more stable μ-oxo diferric complex with the concurrent release of H_2O_2 in solution. For most ferritins, EcBFR being an apparent exception (*41*), the resulting oxo/hydroxo ferric iron ultimately translocates to the interior cavity of the protein where it is stored as a mineral resembling ferrihydrite under phosphate-free conditions (*1,2,4,44*). Translocation of Fe^{3+} is a slow process, typically requiring 24 hr for completion but is greatly assisted by additional incoming Fe^{2+} (*8,12,26*).

In the present study, we investigated the stoichiometries and kinetics of Fe(II) binding, oxidation, and hydrolysis in EcFtnA and site-directed variants of the A-, B-, and C-site ligands to better understand the chemistry of iron oxidation and mineralization and the roles of the various amino acid residues in these processes. The findings reported here confirm and build upon the earlier results from the Harrison laboratory (*10,16,17,25,33,39,58*) and provide new insights into the complex iron chemistry of EcFtnA. The binding and oxidation of an average of 2 Fe^{2+} ions by each of the 24 ferroxidase centers of the protein with a non-integral Fe(II)/O_2 stoichiometry of ~ 3.0 can be explained by the presence of multiple pathways for iron oxidation in the protein involving only the partial reduction of O_2 to H_2O with minimal hydroxyl radical production. Electron paramagnetic resonance (EPR) measurements indicate that a Tyr24 radical is formed following the oxidation of Fe(II) by O_2. Taken together, the present data in conjunction with the literature are consistent with several pathways for iron oxidation in EcFtnA, involving iron at doubly and triply occupied A-, B- and C-sites with both O_2 and H_2O_2 as oxidants. Additionally, iron oxidation directly on the mineral surface occurs as the protein acquires iron and develops a core. The data do not support the hypothesis that the C-site is an essential site, serving as an iron transit site, nor does it support a common mechanism for iron oxidation in all ferritins, as recently suggested (6,7,8,53).

MATERIALS AND METHODS

Recombinant bacterial ferritin (EcFtnA) and its variants were prepared as previously described (*11*) and rendered iron free by anaerobic reduction using 55 mM sodium dithionite in 0.1 M Mes (2-(*N*-morpholino) ethanesulfonic acid), pH 6.0, followed by 5 mM dithionite in the same buffer, each for 3 days. The protein was then dialyzed anaerobically under N_2 against 1 mM 2,2'-dipyridyl in 50 mM Mes, pH 6.0, for 2 days to chelate the Fe(II) produced during the reduction, followed by dialysis against 0.1 M Mes, 0.1 M NaCl, pH 6.0, and finally against the working buffer (*i.e.* 0.1 M Mops, (3-(*N*-morpholino) propanesulfonic acid), 50 mM NaCl, pH 7.0). Protein concentrations were determined spectrophotometrically using the molar absorptivity of 24,000 cm^{-1} M^{-1} at 280 nm for the apoprotein (*11*). All chemicals were of reagent grade and used directly without further purification: ferrous sulfate heptahydrate, $FeSO_4 \cdot 7H_2O$ (J. T. Baker Chemical Co.), Mes and Mops buffers (Research Organics Inc.), 2,2′-dipyridyl and sodium chloride (Aldrich Chemical Co.). The enzyme catalase (EC 1.11.1.6, 65000 units/mg) was purchased from Boehringer-Mannheim GmbH (Germany), the SOD (bovine erythrocyte Cu/Zn SOD) from Sigma-Alrdich Co., the Amplex Red hydrogen peroxide assay kit from Molecular Probes (Eugene, OR) and EMPO from Oxis Research (Portland, OR). The Amplex Red reagent/horseradish peroxidase assay for the measurement of H_2O_2 was performed as described elsewhere (*20*) and employed a standard curve (Fig. S1).

The fluorescence of resorufin, the product of the Amplex Red reagent with hydrogen peroxide was measured at 590 nm using an excitation wavelength of 560 nm on a Cary Eclipse spectrofluorimeter. In the catalase-promoted disproportionation of H_2O_2 ($2H_2O_2 \rightarrow 2H_2O + O_2$), the experiments were performed using a custom made oximetry cell by adding 1 μl of catalase (1300 units) to 0.52 mL of 1.0 μM protein solution in 100 mM Mops, 50 mM NaCl, pH 7.0 either before or after the addition of Fe(II) (Fig. S2). The production of protons was monitored by auto-titration with a standard base (5 mM NaOH)

to maintain the pH at 6.50 with the pH stat apparatus. The use and standardization of the oxygen electrode/pH-stat apparatus are described in detail elsewhere (*26*).

Conventional ultraviolet visible absorbance kinetics was measured at 25 °C on a Varian Cary 50 Bio UV-Vis spectrophotometer with data acquisition every 12.5 ms using a built-in magnetic stirrer and a temperature control Peltier device from Quantum Northwest. The UV-vis dead time for mixing was determined to be ~ 1 s by the jump in absorption at 553 nm from the addition of 5 μL of 6 M NaOH to 1 mL of phenolphthalein solution. Accordingly, the first 1s of data was eliminated from non-linear least-squares fitting of the absorbance-time curves. The Levenberg-Marquardt algorithm and Origin 7.5 software (MicroCal Inc.) were employed in kinetic data analyses. Reactions too fast for the Cary 50 were measured by stopped-flow kinetics at 25 °C as described elsewhere (*12*). All stopped-flow kinetic curves were averages of at least six kinetic traces.

Half-lives ($t_{1/2}$) for iron(II) oxidation were determined from fitting of the first phase of absorbance change at 305 nm on the Cary 50 Spectrophotometer to a rising exponential of the form $A(t) = A[1 – \exp(-\ln(2)t/t_{1/2}]$. Half-lives from 305 nm absorbance-time data were comparable to those obtained from data at ~ 650 nm from Fe(II) oxidation to form the diFe(III) peroxo complex, *e.g.* 120 and 96 ms, respectively for WT EcFtnA measured by stopped-flow. Rate data for the rapidly Fe(II) oxidizing proteins, namely EcFtnA, E49A, Y24F and HuHF, were all determined by stopped-flow for the first 48 Fe(II)/shell addition and analyzed as detailed elsewhere for HuHF (*12*). The kinetics of subsequent additions was sufficiently slow for measurement on the Cary 50 spectrophotometer.

All anaerobic experiments were performed with a thoroughly deoxygenated apo-EcFtnA solution maintained under a constant positive atmosphere of high purity grade argon gas (99.9995%, < 5 ppm O_2). Fluorescence experiments were performed at room temperature on a Varian Cary Eclipse fluorimeter using excitation and emission wavelengths of 280 nm and 330 nm and excitation and emission bandwidths

of 5 nm, respectively. EPR spin-trapping experiments were recorded on a laboratory assembled EPR spectrometer (Bruker ER 041 XK-H) X-band microwave bridge operating at 9.24 GHz with 100 kHz field modulation. Room temperature measurements were performed with a Varian TE_{102} cavity using quartz capillaries having 1 mm inner diameter. Typical spectrometer parameters were: microwave power 5.0 mW; modulation amplitude 0.5 G, time constant 0.3 s; scan rate 7.14 G s^{-1}. In the EMPO spin-trapping experiments for hydroxyl radical, the spectra were recorded immediately after the addition of the last reagent. The experimental conditions are indicated in the figure captions. All data were further analyzed with Origin 7.5 software. EPR measurements of mononuclear iron species and protein radicals were recorded on a Bruker EleXsys E-500 EPR spectrometer using instruments settings as indicated in the figure captions.

RESULTS

Fe^{2+} Binding to EcFtnA

Lack of H^+ production

To determine whether H^+ ions are produced upon Fe^{2+} binding to EcFtnA, different ratios of Fe^{2+} per protein (12, 24, 36 and 48 Fe^{2+}/shell) were added anaerobically to weakly buffered apoprotein at pH 6.5 in 0.3 mM Mes, 100 mM NaCl. Regardless of the amount of iron added, the results indicated no proton release upon Fe^{2+} binding to the apoprotein. The small amount of base delivered to the protein solution following iron addition was equal to a control experiment in which Fe^{2+} was added to the dilute buffer alone (0.3 mM Mes, 100 mM NaCl, pH 6.5). Thus, the equation for Fe^{2+} binding to EcFtnA at pH 6.5 can be written in simplified form as:

$$2\ Fe^{2+} + P^Z \rightarrow [(Fe^{2+})_2\text{-}P]^{Z+4} \qquad (1)$$

where P represents the protein and $[(Fe^{2+})_2\text{-P}]^{Z+4}$ represents a $diFe^{2+}$-protein ferroxidase center complex with Fe^{2+} largely occupying the A- and B-site of the ferroxidase center as observed by anaerobic ITC titration of EcFtnA with Fe^{2+} (*11*).

Fe^{2+} oxidation by O_2 in EcFtnA

Ferroxidase Reaction

As in earlier iron oxidation measurements with different ferritins (*15-18,25,28*), the stoichiometry of Fe^{2+} oxidation in EcFtnA using O_2 as oxidant was followed either by the absorbance increase at 305 nm, due to the formation of oxo/hydroxo $diFe^{3+}$ species at the dinuclear ferroxidase center (Fig. 2A), or by fluorescence quenching (λ_{ex} = 280 nm; λ_{em} = 330 nm) from Tyr19, Tyr24, Phe42 and Phe134 located near the ferroxidase center (Fig. 2B). A stoichiometry of ~ 48 Fe^{3+}/protein shell was obtained in both experiments. Furthermore, when Fe^{2+} was titrated into the same protein sample in increments of 12 Fe^{2+}/shell in the presence of O_2, the initial rates of oxygen consumption and proton production, as measured by oximetry (Fig. 2C) and pH-stat (Fig. 2D), respectively decrease dramatically above 48 Fe^{2+}/protein shell. These data are consistent with the rapid binding and oxidation of an average of two ferrous ions at each ferroxidase center.

The stoichiometries of proton production and oxygen consumption during Fe^{2+} oxidation by O_2 in EcFtnA were measured by pH stat and oximetry. Figure 3 shows the kinetic curves for oxygen consumption and proton production for four successive 12 Fe^{2+}/shell additions at pH 6.5. Replicate measurements on different samples indicate that approximately one proton is generated per Fe^{2+} oxidized (*i.e.* 0.9 ± 0.1 H^+/Fe^{2+}, N = 10) and on average three Fe^{2+} ions are oxidized per oxygen consumed (*i.e.* 3.1 ± 0.2 Fe^{2+}/O_2, N = 10), a value somewhat lower than the stoichiometry of 3.5 Fe(II)/O_2 previously reported (*16*). Similarly, when 48 Fe^{2+}/shell are introduced to the protein in a single addition,

stoichiometries of ~ 3 Fe^{2+}/O_2 and ~ 1 H^+/Fe^{2+} were obtained. The correspondence between the oxygen consumption and proton production curves in Figure 3 indicates that Fe^{2+} oxidation and hydrolysis reactions occur simultaneously within the resolution of the experiment and are coupled to each other.

To test for the production of H_2O_2 during Fe(II) oxidation by O_2, the Amplex Red reagent/horseradish peroxidase assay was employed with three different protein samples in which iron was added in ratios of 24, 48 and 72 Fe^{2+}/shell followed by incubation for 30 minutes at room temperature. Hydrogen peroxide was detected at slightly decreasing levels of 5.7, 5.6 and 5.1 H_2O_2 per 48 Fe^{2+} oxidized for the three Fe^{2+}/shell ratios, respectively. The value of 5.6 ± 0.3 H_2O_2 for 48 Fe(II)/shell sample is considerably less than the 24 H_2O_2 expected for the 2-electron reduction of O_2 expected for the pairwise oxidation of 48 Fe^{2+} at the A- and B-sites. These results are consistent with the consumption of some H_2O_2 produced at the ferroxidase center through the oxidation of Fe^{2+} bound at other ferroxidase centers (more below).

The mineralization reaction

The Fe^{2+}/O_2 and H^+/Fe^{2+} stoichiometries were also determined when Fe^{2+} was added at ratios greater than 48 Fe^{2+}/shell, an amount in excess of that required to saturate the ferroxidase sites in EcFtnA. In the first experiment, 48 Fe^{2+}/shell, or four increments of 12 Fe^{2+}/shell, were added initially to a fresh apoprotein solution and allowed to react to completion before the addition of multiple increments of 48 or 12 Fe^{2+}/shell to the same protein sample. In a second experiment, 200 Fe^{2+}/shell were added at once to the apoprotein and the stoichiometries of Fe^{2+}/O_2 and H^+/Fe^{2+} measured. Below 48 Fe^{2+}/shell, stoichiometries of 2.9 ± 0.2 Fe^{2+}/O_2 and 1.1 ± 0.1 H^+/Fe^{2+} were obtained with iron additions in increments of 12 Fe^{2+}/shell as expected from the ferroxidase experiments described earlier (Fig. 3). When Fe(II) was added in increments of 48 Fe^{2+} /shell to the same protein sample, the oxidation stoichiometry progressively rose

from ~ 3.2 to ~ 3.9 Fe^{2+}/O_2 (Table 1) while the stoichiometry of proton production increased from ~ 1.0 to ~ 2.0 H^+/Fe^{2+} as the total iron accumulated by the protein increased from 48 to 480 Fe^{2+}/shell. From these measured stoichiometries, the net oxidation/mineralization reaction under conditions of high iron loading for WT EcFtnA can be written as follows:

$$4Fe^{2+} + O_2 + 6H_2O \rightarrow 4[FeO(OH)]_{(core)} + 8H^+ \quad (2)$$

where $FeO(OH)_{(core)}$ is a mineral core with UV absorption properties similar to that previously observed with other ferritins (*18,20-22*). Mechanistically, Eq. (2) may be a combination of the following two reactions:

$$2Fe^{2+} + O_2 + 4H_2O \rightarrow 2[FeO(OH)]_{core} + 4H^+ + H_2O_2 \quad (3)$$

$$2Fe^{2+} + H_2O_2 + 2H_2O \rightarrow 2[FeO(OH)]_{core} + 4H^+ \quad (4)$$

The combination of these reactions produces an overall reaction stoichiometry of 4 $Fe(II)/O_2$ and 2 H^+/Fe^{2+} as determined experimentally and expressed in equation 2.

Effect of catalase on the Fe(II)/O_2 stoichiometry

Previous measurements with mammalian ferritins indicated an increase in the stoichiometry of $Fe(II)/O_2$ from ~ 2/1 in the absence of catalase to ~ 4/1 in its presence (*21*). This stoichiometric change was ascribed to H_2O_2 production following Fe(II) oxidation at the ferroxidase center of these proteins and its disproportionation to H_2O and O_2 when catalase is present (*21,29,30*). To further examine the production of H_2O_2 in EcFtnA, catalase was added to an apoprotein solution before the aerobic addition of 48 Fe(II)/shell and the oxygen uptake reaction followed. The presence of catalase increased the observed $Fe(II)/O_2$ stoichiometry from 3.1 to 3.3 (Fig. S2, Curve C). Also, when catalase was added at the end of an experiment following the aerobic addition of either 48 or 72 Fe(II)/shell, some evolution of O_2 occurred, a clear indication of the presence of H_2O_2 in solution (Fig. S2, Curve D), a finding in accord

with the Amplex Red assay described above. Based on the catalase experiments (Fig. S2), 1.9 ± 0.1 H_2O_2 were detected per 48 Fe^{2+} oxidized; this value is considerably lower than that (5.6 ± 0.3 H_2O_2) obtained from the Amplex Red assay. This difference is likely due to the ability of the Amplex Red assay to detect H_2O_2 formed both as an intermediate and as an end product, in contrast to the catalase assay which largely measures H_2O_2 produced as an end product only (*24*).

To test for the possibility that some of the H_2O_2 may have reacted with the iron containing protein, 84 μM H_2O_2 was added directly to a 1 μM holo-EcFtnA protein sample, containing 72 Fe(III)/shell, in 0.1 M Mops (pH 7.4). A slow evolution of O_2 was recorded over a period of 8 min, accounting for ~ 20% of the added H_2O_2, an indication that holo-EcFtnA itself weakly facilitates the disproportionation of H_2O_2 ($H_2O_2 \rightarrow ½\ O_2 + H_2O$), thus accounting for some loss of H_2O_2 in solution. When catalase was added at the end of this experiment, the remaining 80% of H_2O_2 initially added was quantitatively accounted for by the amount of O_2 evolved, a result indicating that the holo-protein itself does not react with hydrogen peroxide. Furthermore, addition of 84 μM H_2O_2 to a 1 μM apoEcFtnA sample in 0.1 M Mops buffer (pH 7.0) produced no measureable O_2, demonstrating that the apoprotein lacks catalase activity and that the presence of iron is required for disproportionation activity. Taken together, the above Amplex Red and catalase experiments indicate that H_2O_2 is produced during the oxidation of Fe^{2+} in EcFtnA by dioxygen and is both an intermediate and an end product. Accordingly, the reactivity of H_2O_2 with Fe^{2+} within EcFtnA was investigated in more detail in order to more fully understand the mechanism of core formation.

Fe^{2+} oxidation by H_2O_2 in EcFtnA

UV-Vis titration and EPR spin-trapping experiments

The oxidation of Fe(II) in EcFtnA by H_2O_2 and the production of hydroxyl radical through the Fenton reaction were examined. Figure 4 (inset) shows a shoulder with an absorbance at ~ 305 nm following H_2O_2 titration (incremental additions of 0.05 H_2O_2/Fe^{2+}) to an anaerobic protein solution containing 48 Fe^{2+}/shell. A stoichiometry of ~ 0.5 H_2O_2/Fe^{2+} was obtained (Fig. 4), indicating that each H_2O_2 oxidizes 2 Fe^{2+} and predicting minimal hydroxyl radical production through the Fenton reaction, *i.e.* $Fe^{2+} + H_2O_2 \rightarrow Fe^{3+} + \cdot OH + OH^-$. In accord with this result, an EPR spin-trapping experiment showed that only a small amount (11% of the control) of hydroxyl radical is produced following the anaerobic addition of H_2O_2 to EcFtnA previously treated with 48 Fe(II)/shell (Fig. 5, spectrum D). In contrast, when H_2O_2 was added to EcFtnA before the addition of Fe(II), a stronger signal of the EMPO-OH adduct was observed corresponding to 42% of that of the control (Fig. 5, spectrum B). This observation indicates that pre-binding of Fe^{2+} to EcFtnA is important in attenuating $HO^{\cdot}$ radical production. In this connection, when more than the stoichiometric amount of iron was added anaerobically to the protein (*i.e.* 72 Fe(II)/shell), the subsequent addition of H_2O_2 gave a stronger EMPO-OH signal corresponding to 31% of the control (Fig. 5, spectrum C). These results indicate that EcFtnA attenuates the generation of hydroxyl radicals as long as stoichiometric amounts of iron have been added to the protein (*i.e.* 2 Fe(II)/subunit) prior to H_2O_2 addition. Most importantly, when 48 Fe(II) were added to the apoprotein aerobically (0.21 atm O_2) in the absence of any added H_2O_2, but otherwise as in Figure 5, no EMPO-OH signal was observed. Only when excess Fe(II) was added (200 Fe(II)/shell) was a small amount of EMPO-OH detected, amounting to only 1.1% of the value of the control on a per iron basis. Thus, EcFtnA is efficient at avoiding Fenton chemistry under normal conditions of aerobic deposition of iron in the protein.

Hydrogen peroxide (24 μM) at a 10-fold lower concentration than O_2 (260 μM), enables EcFtnA-mediated oxidization of 48 Fe(II)/shell at rates 5- to 8-fold faster than obtained with O_2 (Fig. S3A *vs.* Fig. S4A, Table 2) and produces a 305 nm absorbance signal (ε = 3820 $cm^{-1}M^{-1}$ per Fe) comparable to that

with O_2 (3920 $cm^{-1}M^{-1}$ per Fe). The high reactivity of hydrogen peroxide toward Fe(II) in EcFtnA suggests that H_2O_2 produced at one ferroxidase center from the reduction of O_2, can in turn serve as the oxidant of diFe(II) at another center, as found for EcBFR (*20*) and HuHF (12,*21,24*), accounting for consumption of much of the H_2O_2 in solution.

Test for superoxide anion production in EcFtnA and its effect on the Fe(II)/O_2 stoichiometry

To test whether the superoxide anion ($O_2^{\cdot-}$) is formed during iron oxidation by EcFtnA, *in-vitro* spin trapping electron paramagnetic resonance (EPR) was employed. EPR spectra of spin trapped 5-ethoxycarbonyl-5-methyl-1-pyrroline-N-oxide (EMPO) adducts of $O_2^{\cdot-}$ are specific and well described (*54,55*). No EPR spectrum of the EMPO-OOH adducts was observed when Fe(II) was added aerobically to EcFtnA, indicating no detectable superoxide anion in solution and suggesting that the one electron reduction of O_2 through the sole oxidation of mononuclear Fe^{2+} at the C-site does not occur. Thus, Fe^{3+} at the C-site appears to be generated during the simultaneous oxidation of iron at the A-, B- and C-sites as recently proposed based on EPR and Mössbauer data on DvFtn (*48*) and also suggested by earlier work with EcFtnA (*16,17,33*). In accord with the spin trapping results, the measured 3/1 Fe(II)/O_2 stoichiometry in EcFtnA was not altered by the presence of superoxide dismutase.

EPR measurements of C-site mononuclear iron(III) species

Low temperature EPR measurements of mononuclear iron species were undertaken to assess whether mononuclear iron(III) species are formed during iron oxidation in the WT EcFtnA (Procedures for quantifying g' = 4.3 EPR signals of S = 5/2 high spin Fe^{3+} have been detailed elsewhere (*56*)). The EPR spectra of a standard protein sample (a 50% saturated monoferric human serum transferrin) and of three WT EcFtnA samples having 48 or 72 Fe(II)/shell added to 21% O_2 saturated protein solutions were

measured (Fig. S5). Only a relatively weak g = 4.3 signal of mononuclear Fe(III) (S = 5/2) species was obtained with the 48 Fe(III)/shell sample, corresponding to 5.8 ± 0.9 mononuclear Fe(III) per shell and increasing to 6.7 ± 1.0 mononuclear Fe(III) for 72 Fe(II)/shell added. No EPR signal was obtained with the C-site variant E126A, suggesting that the mononuclear Fe(III) is a C-site species, a result in agreement with X-ray structures of C-site variants (*10,33*) and Mössbauer spectra (*17*) showing that the C-site is unoccupied by mononuclear Fe^{3+} in these variants.

Effect of iron-loading on EcFtnA ferroxidase activity

The effect of iron-loading on the ferroxidase activity of EcFtnA and four variants (E49A, E126A, E130A and Y24F) was determined by measurement of the initial rates of iron oxidation from the absorbance change at 305 nm following multiple and successive 48 Fe(II)/protein additions to the same protein sample (Fig. S4). Figure 6A shows the relative initial rates of wild type EcFtnA and its variants normalized to the initial rate obtained for the first 48 Fe(II)/protein addition. A marked decline in rate is observed for all of the proteins following the first addition of 48 Fe(II), *e.g.* 70-fold for the WT protein, in accord with the data in Fig. 2. A marked reduction in absorbance change was also observed after the first addition as shown in Figure 6B ($\varepsilon = 3920\ cm^{-1}M^{-1}$ per Fe for the 1st addition to EcFtnA *vs.* an average of $\varepsilon = 2200\ cm^{-1}M^{-1}$ for additions 2 – 10), an indication of a different environment for the Fe^{3+} after the first 48 Fe addition and different from that of the bulk core ($\varepsilon = 2950\ cm^{-1}M^{-1}$). In these experiments, the time interval between iron additions was 2 to 3 minutes. When longer times were allowed between additions (up to 2 days), complete regeneration of the original ferroxidase activity and original absorbance change upon the first addition was observed in all samples independent of the amount of iron already present within the protein shell. This result suggests that given sufficient time, the ferroxidase centers are vacated by Fe^{3+} to form the thermodynamically more stable mineral core. The C-site variants E49A and E126A

regenerated most of their original ferroxidase activity in a few hours (3-5 hrs), the least amount of time of all the proteins.

The half-lives ($t_{½}$) for Fe(II) oxidation, as determined by measurement of absorbance change at 305 nm for multiple 48 Fe(II) additions (Table 2), show that the A-site variants H53A and E17A and the B-site variant E94A have the slowest rates of oxidation compared to the WT protein and that these variants have minimal ferroxidase activity. The pattern of decreasing half-lives for H53A and, after the first addition for E17A, with increasing number of iron additions follows that expected for an autocatalytic mineral surface reaction, *i.e.* becoming shorter as more iron is added to the protein. The Fe(II)/O_2 stoichiometries of ~ 4/1 for these proteins after a few additions of iron (Table 1) are consistent with a mineral surface reaction (Eq. 2). In contrast, the half-lives for oxidation of the first 48 Fe(II)/shell added to WT EcFtnA, E126A, E49A, E130A and Y24F are comparatively short and correspond to iron oxidation at the ferroxidase centers of the protein where a peroxo-diFe(III) intermediate is produced (*vide infra)*. The longer but highly consistent half-lives for additions 2 – 10 for all these proteins, including HuHF, suggest that the corresponding ferroxidation reactions involve some form of catalysis. However, the increasing Fe(II)/O_2 stoichiometry with increasing Fe(II) additions to EcFtnA (Table 1) clearly indicates that more than one reaction is occurring at comparable rates. The increasing stoichiometry with iron addition to EcFtnA is ascribed to an increasing fraction of the iron being oxidized by H_2O_2 as well as increasing involvement of the mineral surface reaction as previously found for HuHF (*24*).

The addition of two increments of 500 Fe(II) to apoEcFtnA created a biphasic absorbance-time curve (Fig. S6). For the first 500 Fe addition, the rapid first phase has a half-life $t_{1/2}$ = 6.4 s and an absorbance change corresponding to the oxidation of ~ 40 Fe(II)/shell. The second phase has a half-life of 74.8 s that is slow compared to $t_{1/2}$ = 2.4 s with H_2O_2 as the oxidant for 500 Fe(II)/shell (Fig. S3B). Upon addition of a second aliquot of 500 Fe(II)/shell, two phases were again observed but the first phase

corresponds to only about 10 Fe(II)/shell oxidized with an increased half-life from 6.4 to 9.1 s. The second phase gave a 3-fold greater half-life than that of the first 500 Fe(II)/shell addition ($t_{1/2}$ = 232 *vs*. 74.8 s). At this level of added iron (1000 Fe/shell), the mineral surface reaction is presumed to dominate and corresponds to phase 2. Iron oxidation by H_2O_2 at this level of iron is about 135 times faster than by O_2 ($t_{1/2}$ = 1.7 *vs.* 232 s) (Fig. S3B *vs.* S6), again emphasizing the superiority of H_2O_2 over O_2 as an Fe(II) oxidant in EcFtnA.

DiFe(III) Peroxo Complex Formation

Previous stopped-flow measurements demonstrated that a peroxo-diFe(III) intermediate complex is formed during the beginning stages of iron oxidation in EcFtnA and several of its variants (*16,58*); however, a kinetic analysis of the formation and decay of the intermediate(s) was not performed nor were the rate constants reported. Accordingly, the kinetics of oxidation of 48 Fe(II) in EcFtnA, E49A, Y24F and HuHF were measured by stopped-flow and the same fitting equations were applied as developed for the equivalent reaction with HuHF (*12*). As previously shown for HuHF (*12*), the data for EcFtnA (Fig. 7) also conform very well to a sequential reaction scheme of the type $A \xrightarrow{k_1} B \xrightarrow{k_2} B' \xrightarrow{k_2'} C$ where A is a ferrous-dioxygen-protein complex that decays to form the peroxo-diFe(III) complex (species B) which transforms to a related species B' (previously postulated to be a hydroperoxo-diFe(III) complex in HuHF) which then decays to species C, a μ-oxo(hydroxo)-diFe(III) complex. The rate constants determined from curve fitting of the stopped-flow data for the four proteins are summarized in Table 3. Kinetic curves for E49A, Y24F and HuHF are presented in the Supporting Information (Fig. S7). The peroxo complex is formed rapidly in all four proteins but most rapidly in HuHF, k_1 = 31.6 s^{-1} vs. 7.3 s^{-1}, for HuHF and WT EcFtnA, respectively.

To determine whether a peroxo diFe(III) species is also formed when 48 Fe(II)/shell are added to the holoprotein, a sample was prepared by the addition of 72 Fe(II) to the apoprotein, enough to saturate the

A-, B- and C-sites of all 24 subunits. The freshly prepared sample was then rapidly mixed with 48 Fe(II)/shell in the stopped-flow apparatus. Only a relatively weak broad absorbance at ~ 650 nm was observed compared to the same experiment with the apoprotein where a maximal absorbance occurred at ~ 610 nm (Fig. S8). The absorbance at 650 nm rapidly increased then declined relatively slowly in a manner resembling the formation and subsequent decay of an intermediate, presumably also a peroxo-diFe(III) complex or related species (Fig. S9). The value ($k_1 \sim 6\ s^{-1}$) of the rate constant for the rapid first phase formation of this intermediate in the holoprotein is comparable to the value of $k_1 = 7.3\ s^{-1}$ for the apoprotein (Fig. 7, Table 3). When the kinetics of the holoprotein and apoprotein are compared at 310 nm, the first phase for the holoprotein has a k_1 of $\sim 8\ s^{-1}$ but an amplitude that is only about 10% as large as that of the first phase ($k_1 \sim 7\ s^{-1}$) of the apoprotein (Fig. S10). These data (Figs. S8 and S9) indicate limited regeneration of the peroxo complex at an Fe(II) to EcFtnA ratio greater than 72, which contrasts with HuHF where continual regeneration of the peroxo complex is observed in the presence of excess Fe(II), beyond that required to saturate the ferroxidase centers (*12,53*). The iron uptake curves for the apoprotein and holoprotein are also quite different (Fig. S10), indicating distinct mechanisms, in accord with the results in Figs. 2 and 6, and Tables 2 and 3. We conclude that the production of the observed "peroxo-diFe(III)" species in the holoprotein represents a relatively minor reaction that involves either a few remaining unoccupied ferroxidase centers or the displacement of Fe(III) by incoming Fe(II) from a small subset of centers.

Tyrosyl radical formation

Previous EPR studies have revealed the production of a tyrosyl radical during iron oxidation in human H-chain ferritin which was assigned to Tyr34 located adjacent to the ferroxidase center (*32*). Because in EcFtnA Tyr-24 is located only about 2.5 Å from the B-site of the diiron nuclear center, EPR spectroscopy

was employed to examine whether a tyrosyl radical likewise is formed in EcFtnA. The EPR spectrum (Fig. 8) of a frozen solution at 77K following the aerobic addition of 48 Fe^{2+}/shell to the WT protein in Mops buffer at pH 7.0 shows features similar to those of tyrosyl radicals in human H-chain and horse spleen ferritins, and also to known tyrosine radicals in a number of enzymes (*32,57*). When the protein sample was allowed to stand at room temperature, the EPR signal decayed with a half-life of 4.3 min (Fig. 8, inset). The lack of any spectral broadening when the reaction was carried out with $^{57}Fe^{2+}$ argues against this species being an iron-coupled radical. It is easily power saturated ($P_{1/2}$ = 0.71 ± 0.5 mW) (Fig. S11). The EPR signal is absent in variant Y24F and also in A-site variants His53A and E17A, B-site variant E94A, A- and B-site variant E50A and in B- and C-site variant E130A. In contrast, the two C-site variants E126A and E49A showed the tyrosine radical EPR signal but of attenuated intensity, ~ 40 and 60 % that of the WT, respectively. Collectively, these observations strongly suggest that the radical is centered on Tyr24 and that fully functional A and B-sites, but not the C-site, are required for its generation.

DISCUSSION

The present work reveals several new properties of EcFtnA and confirms and expands on findings of previous studies (*10,11,16,17,25,33,39*). In many respects, EcFtnA displays iron oxidation properties similar to those of HuHF. Both exhibit Fe(II) oxidation stoichiometries of 48 Fe^{2+}/shell (Fig. 2; *21,24,26,27*), display H_2O_2 detoxification properties whereby two Fe^{2+} are oxidized per H_2O_2 reduced (Fig. 5), require fully functional A- and B-sites for high ferroxidase activity (Table 2) (*2-4*), produce two related colored reaction intermediates (Fig. 7) (*12*) and both generate a tyrosyl radical (Fig. 8) (*32*). However, EcFtnA differs from HuHF in having an Fe(II)/O_2 oxidation stoichiometry of ~3 vs ~2 for HuHF (*26,30*) for the first 48 Fe(II) added to the protein.

Elimination of either A- or B-site ligands of EcFtnA, as in variants H53A, E17A and E94A, increases the Fe(II)/O_2 stoichiometry from ~ 3 to ~ 4 (Table 1). The half-life for iron oxidation for the first 48 iron addition also increases markedly for these variants compared to that of the WT protein but then begins to shorten with subsequent additions of Fe(II) to H53A and E17A (Table 2). These properties are hallmarks of a largely autocatalytic mineral surface driven reaction (eq. 2) as expected for a ferritin with a largely disabled ferroxidase center.

The C-site is a common feature of many bacterial ferritins. The amino acid sequences of five ferritins (*Helicobacter pylori*, HpF; *Archaeoglobus fulgidus*, AfFtn; *Pyrococcus furiosus*, PfFtn; *Desulfovibrio vulgaris*, DvFtn and *Escherichia coli,* EcFtnA) all show highly conserved C-site residues, suggesting an important function of this site (*33-39,48*). Indeed, the C-site of EcFtnA is not a passive player in the ferroxidase activity of the protein but rather modulates the stoichiometric and kinetic properties of the protein. Elimination of C-site ligands as in variants E126A, E49A and E130A causes a decrease in the Fe(II)/O_2 stoichiometry from ~3 to ~ 2 for the first 48 Fe(II) added to the protein (Table 1) (*16*), giving these proteins the same stoichiometry as HuHF with its putative weakly complexing C-site (*7*). Moreover, C-site variants (particularly E49A and E126A) fully regenerated their initial ferroxidase activity within a few hours, as was found in an earlier Mössbauer spectroscopic study (*17*), compared to a day or so required for WT EcFtnA (Results) (*17*). The E49A C-site mutation of EcFtnA also causes all three rate constants (k_1, k_2 and k_2') for the formation and decay of the peroxo intermediates to shift toward the values of HuHF, in effect making EcFtnA more "HuHF-like" in its kinetic properties (Table 3). The above findings are in accord with ITC titrations of Fe^{2+} binding to EcFtnA and its variants showing a strong interplay between the C-site and the A- and B-sites (*11*).

The strong effect of mutation of C-site ligands of EcFtnA on the iron oxidation reactions (Tables 1-3) is consistent with the observation that the blue diferric peroxo intermediate seen in WT EcFtnA

increases in intensity in C-site variants E49A, E126A and E130A (*16,58*) where more of the bound iron is expected to participate in peroxo complex formation at the A and B-sites (*33*). Thus, the oxidation stoichiometry of 48 Fe(III)/shell reported above with WT EcFtnA likely reflects the existence of some EcFtnA molecules with all three sites (A-, B- and C-sites) occupied by iron while others are metal free or have only A- and B-sites occupied as previously proposed (*10,25,48*). (If all three sites were occupied on all 24 subunits, a binding stoichiometry of 72 Fe(III)/shell would be expected but this is contrary to observation (Fig. 2)). These results suggest negative cooperativity in the binding of iron to different subunits. Quantitative EPR measurements on the g' = 4.3 signal indicates that approximately 6 mononuclear C-site Fe^{3+} are present per protein shell following oxidation of 48 Fe^{2+} (Results). If Fe^{3+} in the C-site is only formed simultaneously with the oxidation of iron in the A- and B-sites as Mössbauer data suggest (*17*), then approximately 6 ferroxidase centers with triply occupied sites are present in the protein samples of this work. Eventually all sites become occupied and the core begins to form as further iron is added to the protein (*17*).

In previous work, it has been suggested that oxidation of some Fe(II) in the C-site has the benefit of helping to avoid reactive oxygen species (*16*), a suggestion in agreement with the spin trapping results and limited production of H_2O_2 reported here. Moreover, it has also been proposed that iron being retained in the site of oxidation may be more available to the cell than core iron during iron mobilization (*16*). It is worth noting that the C-site in HuHF is composed of Glu140 (*7*) (Glu126 in EcFtnA); however, the C-site residues Glu129 and Glu130 in EcFtnA are replaced by Lys and Ala, respectively, in HuHF, so the site is not highly conserved. Moreover, the mutations E140A and E140Q in HuHF reduce the rate of oxidation by only ~ 50% (*7*), not a large effect if the C-site were essential for function. In contrast, the mutations E129R, E129C and E129Q in PfFtn reduce the rate of oxidation by more than 10-fold (*8*) in accord with an important role for Glu129 in this protein. The same mutation in

soybean ferritin has only a modest effect on the kinetic parameters, decreasing the rate of iron oxidation - mainly through a 2.2-fold increase in K_m with little effect on V_{max} and k_{cat} (6). In the case of EcFtnA, the C-site mutation E49A has a limited effect on the kinetics (Tables 2 and 3) whereas the C-site variant E126A displays significantly reduced rates (Table 2). Thus, the findings regarding the effect of C-site ligands on iron oxidation in ferritins from different sources are mixed, require further investigation and presently do not imply a common function for all ferritins.

One of the unique properties of EcFtnA is its unusual Fe(II)/O_2 oxidation stoichiometry of ~ 3. It seems unlikely that the stoichiometry is simply due to oxidation of the protein as reflected by the observed tyrosine radical (Fig. 8) because such a radical is also observed in HuHF (*32*) which has Fe(II)/O_2 of ~ 2 (*21,24,26,30*) . Furthermore, while elimination of Tyr24 through the mutation Y24F affects the Fe(II)/O_2 stoichiometry, reducing it from 3.1 to 2.4, the Tyr radical is still observed in C-site variants E49A and E126A having Fe(II)/O_2 stoichiometries of ~ 2 (Table 1) as in HuHF. The tyrosine radical observed here conceivably arises from radical damage to the protein as found for other ferritins (*46,60,61*). We also note that variant Y24F itself is a kinetically competent protein capable of forming a diFe(III) peroxo complex (*16,58*) upon addition of the first 48 Fe(II) to the protein with rate parameters similar to WT EcFtnA (Fig. S7B, Table 3). However, with subsequent additions of 48 Fe(II) to Y24F, the half-lives for oxidation are about 4-fold longer than those of the WT EcFtnA (Table 2), suggesting a possible redox or structural role for Tyr24 as the protein begins to build the core . The effect of the mutation Y24F on the kinetics has been previously attributed to the hydrogen bond of Tyr24 to Glu94 of the B-site (Fig. 1), the B-site being essential for iron oxidation, and thus intimately involved in the structure of the ferroxidase center (*16,33,34,45*). However, we emphasize that a redox role for Tyr24 in EcFtnA is not excluded by the present data.

A transient radical assigned to a Tyr24 radical has recently been reported for PfFtn (*53*) with similar fine structure to that seen here for EcFtnA (Fig. 8). Despite the similar structures and metal site homologies of EcFtnA and PfFtn (*10,33,34*), the radical in PfFtn has a short chemical lifetime ($t_{1/2}$ ~ 2 s compared to 4.3 min for EcFtnA (Fig. 8, inset) and cannot be observed above 50 K , a property attributed to the proximity of the radical to the paramagnetic iron of the ferroxidase center (*53*). In contrast, the radical spectrum of EcFtnA reported here (Fig. 8) is readily observable at 77 K, easily power saturates and lacks ^{57}Fe hyperfine structure. Thus, it does not appear to be in close proximity to Fe^{3+} and may arise from a radical located at ferroxidase centers in EcFtnA which have been vacated of their complement of Fe^{3+}. Whether a more transient radical than the Tyr24 radical reported here also exists in EcFtnA as seen in PfFtn (*53*) and in HoSF (59) by freeze-quench EPR remains to be determined. A more transient Tyr24 radical could play a role in facilitating Fe(II) oxidation beyond the first 48 Fe added to the protein and may account for increased half-lives observed for variant Y24F relative to WT EcFtnA after the first addition of 48 Fe(II) (Table 2).

Hagen and coworkers, based on extensive experimental work with PfFtn and HuHF, have proposed a common mechanism for all ferritins whereby iron is oxidized by two catalytic pathways (*8,53*). In the first pathway, iron is oxidized at the A- and B-sites of the ferroxidase center and H_2O_2 is the product of dioxygen reduction, giving an Fe(II)/O_2 stoichiometry of 2/1. For simplicity, we have omitted water and the sources of protons in the illustration of this first pathway, *viz.,*

$$Fe_A^{2+}Fe_B^{2+} + O_2 \rightarrow [Fe_A^{3+}(O_2^{2-})Fe_B^{3+}]_{peroxo} \rightarrow (Fe_A^{3+}(OH^-)_2 Fe_B^{3+}) + H_2O_2 \qquad \text{(Pathway 1)}$$

The first pathway is the generally accepted one in the literature for HuHF (*2,12,13,21,24,26*). In the second pathway, iron is simultaneously oxidized at the A-, B- and C-sites of the ferroxidase center along with Tyr24 to form a Tyr cation radical $Y^{\bullet+}$ that is subsequently neutralized by oxidation of additional Fe^{2+} at an unspecified site to give a net Fe(II)/O_2 stoichiometry of 4/1, *viz.*

$$Fe_A^{2+}Fe_B^{2+}Fe_C^{2+}Y + O_2 \rightarrow [Fe_A^{3+}(O_2^{2-})Fe_B^{3+}Fe_C^{2+}Y]_{peroxo} \rightarrow [Fe_A^{3+}(OH^-)_2Fe_B^{3+}Fe_C^{3+}Y^{\bullet+}]$$

$$Y^{\bullet+} + Fe^{2+} \rightarrow Y + Fe^{3+} \qquad \text{(Pathway 2)}$$

Zn^{2+} binding sites at His93 and His128 identified in the crystal structure of EcFtnA have been suggested as possible additional Fe^{2+} oxidation sites (*33*).

We now consider the two pathway model in terms of the amount of H_2O_2 detected in solution and the observed Fe(II)/O_2 stoichiometry. If the stoichiometry S = Fe(II)/O_2 is determined by only the above two pathways having stoichiometries of 2/1 and 4/1, respectively, the measured value would be given by $1/S = 1/2 \bullet X_1 + 1/4\, X_2 = 1/2 \bullet X_1 + 1/4 \bullet (1 - X_1)$ where X_1 and X_2 are the mole fractions of iron oxidized by the two pathways, respectively. Given that S = 3.1 ± 0.2, we obtain X_1 = 0.29 ± 0.08 and X_2 = 0.79 ± 0.08 or about 1/3 of the iron is processed by Pathway #1 and 2/3 by Pathway #2, or 13.9 Fe and 34.1 Fe by the two pathways, respectively. For every two Fe atoms that proceed by Pathway #1, one H_2O_2 is produced. Thus this model predicts that 7.0 ± 1.9 H_2O_2 $(13.9 \div 2)$ would be produced if only these two pathways were operable, a value far larger than the value of 1.9 ± 0.1 H_2O_2 observed experimentally using catalase to measure the end product H_2O_2 (Results, Fig. S2). Obviously, some of the 5.6 ± 0.3 H_2O_2 detected as an intermediate by the Amplex Red assay has reacted further. The much faster oxidation of Fe(II) by H_2O_2 compared to O_2 for all levels of iron added (Results; Figs. S3, S4A and S6), the Fe(II)/H_2O_2 stoichiometry of 2 (Fig. 4) and minimal hydroxyl radical production (Fig. 5) imply that some iron almost certainly is oxidized by H_2O_2 in a pairwise fashion, either at the ferroxidase center, namely $Fe_A^{2+}Fe_B^{2+} + H_2O_2 \rightarrow (Fe_A^{3+}(OH^-)_2Fe_B^{3+})$ or on the mineral surface (Eq. 4). Also, some disproportionation of H_2O_2 ($H_2O_2 \rightarrow$ ½ O_2 + H_2O) occurs to a small extent, but this is a slow process (Results), and cannot account for most of the H_2O_2 consumed.

The data for EcFtnA deviates from that of PfFtn in several significant ways despite their sequence similarity, identical metal ligands and similar Fe(II)/O_2 oxidation stoichiometries of ~ 3/1. Integral to

the proposed "unified mechanism" is the essential roles of the C-site and tyrosine radical (*6-8,53*) which clearly are not required for rapid iron oxidation in EcFtnA as studies with the variants indicate (Tables 2 and 3) and others have found (*19,11,16,17,25,33,39*). EcFtnA readily acquires iron without an intact C-site or the presence of Tyr24 (*16,17,25,33,39*). Furthermore, while the x-ray structure of EcFtnA (*10,33*) and Mössbauer spectroscopy (*17,25*) show iron(III) occupancy of the A-, B- and C-sites and no iron core following oxidation of 48 Fe(II), the data indicate that a second addition of 48 Fe(II) displaces little or none of the first 48 Fe from the A-, B- and C-sites but rather mostly fills vacant sites and builds the core (*17*), a finding inconsistent with the proposal that the C-site is a transit site (*6-8,53*). Our observation of only a weak signal from a peroxo diFe(III) intermediate when 48 Fe^{2+} are rapidly mixed with a freshly prepared holoEcFtnA containing 72 Fe^{3+}, essentially filling the A, B and C sites (*17*) (Figs. S8-S10) is consistent with the Mössbauer findings, namely that iron does not appreciably turnover at the ferroxidase center (*17*). The rapid phase of the kinetics when 48 Fe(II) are added to the holoprotein containing 72 Fe(II) being only ~10% of that seen when 48 Fe(II) are added to the apoprotein (Fig. S10) further argues against significant turnover of iron at the ferroxidase center in the time frame of minutes. Finally, we note that the Fe^{2+} binding isotherms measured by ITC are very different in appearance for PfFtn (*8*) and EcFtnA (*11*). PfFtn shows one strong highly exergonic and two weak highly endergonic binding sites per subunit compared to EcFtnA which exhibits two strong slightly endergonic binding sites per subunit plus some undefined weak binding.

What then is the origin of the catalytic activity of EcFtnA given that there is limited turnover of Fe(III) at the A-, B- and C-sites in the short time frame of our experiments? Clearly the ferroxidase center is essential for catalytic activity for iron additions beyond the first 48 Fe(II) added because mutation of A- or B-site ligands largely abolishes activity and mutation of C-site ligands modifies activity (Table 2). One possibility is that once the ferroxidase center of EcFtnA is saturated with iron,

iron occupancy of the C-site inhibits iron turnover at the A- and B-sites so that they serve as a redox cofactor as proposed for EcBFR (*40,41*). In any case, EcFtnA efficiently oxidizes iron at a pace that is comparable to that of HuHF (Table 2) even though iron displacement from the ferroxidase center appears to be minimal in EcFtnA (*17,33*) but occurs in HuHF (*8,12*). Our data in conjunction with the literature indicate that the mechanism of iron oxidation and deposition in EcFtnA is complex with multiple reactions involving the A-, B- and C-sites of the ferroxidase center, the mineral surface and both O_2 and H_2O_2 as oxidants.

Supporting information available. Amplex Red standard curve; effects of catalase on oxygen consumption curves of EcFtnA, absorbance-time kinetic curves at 305 nm for Fe(II) oxidation in WT EcFtnA by hydrogen peroxide with iron added in increments of 48 or 500 Fe(II)/shell; absorbance-time kinetic curves for Fe(II) oxidation by dioxygen in WT EcFtnA, H53A, E17A, E94A, E130A, E49A, E126A, Y24F, and HuHF with iron added in increments of 48 Fe(II)/shell; absorbance-time stopped-flow curves at 585-650 nm for diFe(III) peroxo complex formation and decay in E49A, Y24F and HuHF and corresponding curve fits; multiwavelength stopped-flow spectra for 48 Fe(II)/shell addition to apoEcFtnA and holoEcFtnA; absorbance-time stopped-flow curves at 650 nm and 310 nm for 48 Fe(II) added to holoEcFtnA containing 72 Fe(III); g'=4.3 EPR spectra of EcFtnA; and EPR power saturation curves of Tyr24 radical. This material is available free of charge via the internet at http://pubs.acs.org.

REFERENCES

1. Andrews, S. C. (1998) Iron storage in bacteria. *Adv. Microb. Physiol. 40*, 281-351.

2. Chasteen, N. D., and Harrison, P. M. (1999) Mineralization in ferritin: An efficient means of iron storage. *J. Struct. Biol. 126*, 182-194.

3. Chasteen, N. D. (1998) Ferritin. Uptake, storage, and release of iron, in *Metal Ions in Biological Systems,* Vol. 35, (Sigel, H. and Sigel, A., Eds.), pp 479-514, Marcel Dekker Inc., New York,

4. Harrison, P. M., and Arosio, P. (1996) The ferritins: Molecular properties, iron storage function and cellular regulation. *Biochim. Biophys. Acta* 1275, 161-203.

5. Bou-Abdallah, F., Biasiotto, G., Arosio, P., and Chasteen, N. D. (2004) The putative nucleation site in human H-chain ferritin is not required for mineralization of the iron core. *Biochemistry 43*, 4332-4337.

6. Matsuda, T., Goto, F., Yoshhara, T., and Mikami, B. (2010) Crystal structure of plant ferritin reveals a novel metal binding site that functions as a transit site for metal transfer in ferritin, *J. Biol. Chem. 285*, 4049-4059.

7. Matsuda, T., Goto, F., Yoshhara, T., and Mikami, B. (2010) The universal mechanism for iron translocation to the ferroxidcase site in ferritin, which is mediated by the well conserved transit site, *Biochem. Biophys. Res. Commun. 400*, 94-99.

8. Ebrahimi, K. H., Bill, E., Hagedoorn, P.-L., and Hagen, W. R. (2012) The catalytic center of ferritin regulates iron storage via Fe(II)-Fe(III) displacement, *Nat. Chem. Biol. 8*, 941-948.

9. Harrison, P. M., Hempstead, P. D., Artymiuk, P. J., and Andrews, S. C. (1998) Structure-function relationships in the ferritins. in *Metal Ions in Biological Systems,* Vol. 35, (Sigel, H. and Sigel, A., Eds.), pp 435-477, Marcel Dekker, Inc., New York,.

10. Stillman T.J., Hempstead P.D., Artymiuk P.J., Andrews S.C., Hudson A.J., Treffry A, Guest J.R., and Harrison P.M. (2001) The high-resolution X-ray crystallographic structure of ferritin (EcFtnA) of

Escherichia coli; Comparison with human H ferritin (HuHF) and the structures of the Fe(3+) and Zn(2+) derivatives. *J. Mol. Biol. 307*, 587–603.

11. Bou-Abdallah, F., Woodhall, M. R., Velásquez-Campoy, A., Andrews, S. C., and Chasteen, N. D. (2005) Thermodynamic analysis of ferrous ion binding to *Escherichia coli* ferritin EcFtnA. *Biochemistry 44,* 13837-13846.

12. Bou-Abdallah, F., Zhao, G., Mayne, H. R., Arosio, P., and Chasteen, N. D. (2005) Origin of the unusual kinetics of iron deposition in human H-chain ferritin. *J. Am. Chem. Soc. 127*, 3885-3893.

13. Bou-Abdallah, F., Papaefthymiou, G., Scheswohl, D., S., Stanga, S., Arosio, P., and Chasteen, N. D. (2002) μ-1,2-Peroxobridged di-iron(III) dimer formation in human H-chain ferritin. *Biochem. J. 364*, 57-63.

14. Zhao, G., Su, M., and Chasteen, N. D. (2005) μ-1,2-peroxo diferric complex formation in horse spleen ferritin. A mixed H/L-subunit heteropolymer. *J. Mol. Biol. 352*, 467–477.

15. Moenne-Loccoz, P., Krebs, C., Herlihy, K., Edmondson, D. E., Theil, E. C., Huynh, B. H., and Loehr, T. M. (1999) The ferroxidase reaction of ferritin reveals a diferric μ-1,2 bridging peroxide intermediate in common with other O_2-activating non-heme diiron proteins. *Biochemistry* 38, 5290-5295.

16. Treffry, A., Zhao, Z, Quail, M. A., Guest, J. R., and Harrison, P. M. (1998) How the presence of three iron binding sites affects the iron storage function of the ferritin (EcFtnA) of *Escherichia coli*. *FEBS Letts. 432*, 213-218.

17. Bauminger, E. R., Treffry, A., Quail, M. A., Zhao, Z. W., Nowik, I., and Harrison, P. M. (1999) Stages in iron storage in the ferritin of *Escherichia coli* (EcFtnA): analysis of Mössbauer spectra reveals a new intermediate. *Biochemistry 38*, 7791-7802.

18. Bou-Abdallah, F., Santambrogio, P., Levi, S., Arosio, P., and Chasteen, N. D. (2005) Unique iron binding and oxidation properties of human mitochondrial ferritin: A comparative analysis with human H-chain ferritin. *J. Mol. Biol. 347*, 543-554.

19. Pereira, A. S., Small, W., Krebs, C., Tavares, P., Edmondson, D. E., Theil, E. C., and Huynh, B. H. (1998) Direct spectroscopic and kinetic evidence for the involvement of a peroxodiferric intermediate during the ferroxidase reaction in fast ferritin mineralization. *Biochemistry 37*, 9871-9876.

20. Bou-Abdallah, F., Lewin, A. C., Le Brun, N. E., Moore, G. R., and Chasteen, N. D. (2002) Iron detoxification properties of *Escherichia coli* bacterioferritin: Attenuation of oxyradical chemistry. *J. Biol. Chem. 277*, 37064-37069.

21. Zhao, G., Bou-Abdallah, F., Yang, X., Arosio, P., and Chasteen, N. D. (2001) Is hydrogen peroxide produced during iron(II) oxidation in mammalian apoferritins? *Biochemistry 40*, 10832-10838.

22. Yang, X., Le Brun, N. E., Thomson, A. J., Moore, G. R., and Chasteen, N. D. (2000) The iron oxidation and hydrolysis chemistry of *Escherichia coli* bacterioferritin. *Biochemistry 39*, 4915-4923.

23. Pereira, A. S., Tavares, P., Lloyd, S. G., Danger, D., Edmondson, D. E., Theil, E. C., and Huynh, B. H. (1997) Rapid and parallel formation of Fe^{3+} multimers, including a trimer, during H-type subunit ferritin mineralization. *Biochemistry 36*, 7917-7927.

24. Zhao, G., Bou-Abdallah, F., Arosio, P., Levi, S., Janus-Chandler, C., and Chasteen, N. D. (2003) Multiple pathways for mineral core formation in mammalian apoferritins. The role of hydrogen peroxide. *Biochemistry 42*, 3142-3150.

25. Bauminger, E. R., Treffry, A., Quail, M. A., Zhao, Z., Nowik, I., and Harrison, P. M. (2000) Metal binding at the active centre of the ferritin of *Escherichia coli* (EcFtnA). A Mössbauer spectroscopic study. *Inorg. Chim. Acta 297*, 171-180.

26. Yang, X., Chen-Barrett, Y., Arosio, P., and Chasteen, N. D. (1998) Reaction paths of iron oxidation and hydrolysis in horse spleen and recombinant ferritins. *Biochemistry 37*, 9743-9750.

27. Treffry, A., Zhao, Z, Quail, M. A., Guest, J. R., and Harrison, P. M. (1997) Dinuclear center of ferritins: Studies of iron binding and oxidation show differences in the two iron sites. *Biochemistry 36*, 432-441.

28. Jameson, G. N. L., Jin, W., Krebs, C., Pereira, A. S., Tavares, P., Liu, X., Theil, E. C., and Huynh, B. H. (2002) Stoichiometric production of hydrogen peroxide and parallel formation of ferric multimers through decay of the diferric-peroxo complex, the first detectable intermediate in ferritin mineralization. *Biochemistry 41*, 13435-13443.

29. Sun, S., and Chasteen, N. D. (1992) Ferroxidase kinetics of horse spleen apoferritin. *J. Biol. Chem. 267*, 25160-25166.

30. Xu, B., and Chasteen, N. D. (1991) Iron oxidation chemistry in ferritin. Increased Fe/O_2 stoichiometry during core formation. *J. Biol. Chem. 266*, 19965-19970.

31. Bunker, J., Lowry, T., Davis, G., Zhang, B., Brosnahan, D., Lindsay, S., Costen, R., Choi, S., Arosio, P., and Watt, G. D. (2005) Kinetic studies of iron deposition catalyzed by recombinant human liver heart, and light ferritins and *Azotobacter vinelandii* bacterioferritin using O_2 and H_2O_2 as oxidants. *Biophys. Chem. 114*, 235– 244.

32. Chen-Barrett, Y., Harrison, P. M., Treffry, A., Quail, M. A., Arosio, P., Santambrogio, P., and Chasteen, N. D. (1995) Tyrosyl radical formation during the oxidative iron deposition in the human apoferritin. *Biochemistry 34*, 7847-7853.

33. Stillman, T. J., Connolly, P. P., Latimer, C. L., Morland, A. F., Quail, M. A, Andrews, S. C., Treffry, A., Guest, J. R., Artymiuk, P. J., and Harrison, P. M. (2003) Insight into the effects on metal binding of

the systematic substitution of five key glutamate ligands in the ferritin of *Escherichia coli*. *J. Biol. Chem. 278,* 26275–26286.

34. Tatur, J., Hagen, W. R. and Matias, P.M. (2007) Crystal structure of the ferritin from the hyperthermophilic archaeal anaerobe *Pyrococcus furiosus*. *J. Biol. Inorg. Chem. 12*, 615–630.

35. Cho, K. J., Shin,H. J., Lee, J. H., Kim, K. J., Park, S. S., Lee, Y., Lee, C., and Kim, K. H. (2009). The crystal structure of ferritin from *Helicobacter pylori* reveals unusual conformational changes for iron uptake, *J. Mol. Biol. 390*, 83–98.

36. Ebrahim, K.H., Hagedoorn, P.-L., Jongejan, J. A., and Hagen, W. R. (2009) Catalysis of iron core formation in Pyrococcus furiosus ferritin. *J. Biol. Inorg. Chem. 14*, 1265-1274.

37. Johnson, E., Cascio, D., Sawaya, M.R., Gingery, M., and Schröder, I. (2005) Crystal Structures of a Tetrahedral Open Pore Ferritin from the Hyperthermophilic Archaeon *Archaeoglobus fulgidus*. *Structure 13*, 637-648.

38. Nick E. Le Brun, Allister Crow, Michael E.P. Murphy, A. Grant Mauk, Geoffrey R. Moore (2010). Iron core mineralisation in prokaryotic ferritins. *Biochimica et Biophysica Acta 1800,* 732–744

39. Treffry, A., Zhao, Z, Quail, M. A., Guest, J. R., and Harrison, P. M. (1998) The use of zinc(II) to probe iron binding and oxidation by the ferritin (EcFtnA) of *Escherichia coli*. *J. Biol. Inorg. Chem. 3*, 682-688.

40. Baaghil, S., Lewin, A., Moore, G. R., and Le Brun, N. E. (2003) Core formation in Escherichia coli bacterioferritin requires a functional ferroxidase center. *Biochemistry 42*, 14047–14056.

41. Crow, A., Lawson, T. L., Lewin, A., Moore, G. R., and Le Brun, N. E. (2009) Structural basis for iron mineralization by bacterioferritin. *J. Am. Chem. Soc. 131*, 6808–6813.

42. Lawson, T. L., Crow, L., Lewin, A., Yasmin, S., Moore, G. R., and Le Brun, N. E. (2009) Monitoring the iron status of the ferroxidase center of Escherichia coli bacterioferritin using

fluorescence spectroscopy. *Biochemistry 48*, 9031–9039.

43. Bou-Abdallah, F., Carney, E., Chasteen, N. D., Arosio, P., Viescas, A. J., and Papaefthymiou, G. C. (2007) A comparative Mössbauer study of the mineral cores of human H-chain ferritin employing dioxygen and hydrogen peroxide as iron oxidants. *Biophys. Chem. 130*, 114–121.

44. Bou-Abdallah, F. (2010) The iron redox and hydrolysis chemistry of the ferritins. *Biochimica et Biophysica Acta 1800*, 719–731.

45. Fetter, J., Cohen, J., Danger, D., Sanders-Loehr, J., and Theil, E.C. (1997) The influence of conserved tyrosine 30 and tissue-dependent differences in sequence on ferritin function: use of blue and purple Fe(III) species as reporters of ferroxidation, *J. Biol. Inorg. Chem. 2*, 652-661.

46. Bellapadrona, G., Ardini, M., Ceci, P., Stefanini, S., and Chiancone, E. (2010) Dps proteins prevent Fenton mediated oxidative damage by trapping hydroxyl radicals within the protein shell. *Free Radic Biol Med. 48*:292-297.

47. Zhao, G., Arosio, P., and Chasteen, N. D. (2006) Iron(II) and hydrogen peroxide detoxification by human H-chain ferritin. An EPR spin-trapping study. *Biochemistry 45,* 3429-3436.

48. Pereira, A. S., Timóteo, C. G., Guilherme, M., Folgosa, F., Naik, S. G., Duarte, A. G., Huynh, B. H., and Tavares, P. (2012) Spectroscopic evidence for and characterization of a trinuclear ferroxidase center in bacterial ferritin from *Desulfovibrio vulgaris* Hildenborough, *J. Am. Chem. Soc. 134*, 10822-10832.

49. Lowery, T. J., Bunker, J., Zhang, B., Costen, R., and Watt G. D. (2004) Kinetic studies of iron deposition in horse spleen ferritin using H_2O_2 and O_2 as oxidants. *Biophys. Chem*. *111*, 173–181.

50. Su, M., Cavallo, S., Stefanini, S., Chiancone, E., and Chasteen, N. D. (2005) The so-called *Listeria innocua* ferritin is a Dps protein, iron incorporation, detoxification, and DNA protection properties. *Biochemistry 44,* 5572-5578.

51. Liu, X., Kim, K., Leighton, T., and Theil, E. C. (2006) Paired *Bacillus anthracis* Dps (mini-ferritin) have different reactivities with peroxide. *J. Biol. Chem. 281*, 27827–27835.

52. Wiedenheft, B., Mosolf, J., Willits, D., Yeager, M., Dryden, K. A., Young, M., and Douglas, T. (2005) An archaeal antioxidant: characterization of a Dps-like protein from Sulfolobus solfataricus. *Proc. Natl. Acad. Sci. 102*,10551–10556.

53. Ebrahimi, K. H., Hagedoorm, P.-L. and Hagen, W. R. (2013) A conserved tyrosine in ferritin is a molecular capacitor, *ChemBioChem14*, 1123-1133.

54. Zhang, H., Joseph, J., Vasquez-Vivar, J., Karoui, H., Nsanzumuhire, H., Martásek, P., Tordo, P., and Kalyanaraman, B. (2000) Detection of superoxide anion using an isotropically labeled nitrone spin trap: Potential biological applications. *FEBS Lett. 473*, 58–62.

55. Bou-Abdallah, F., Chasteen, N. D., and Lesser, M. P. (2006) Quenching of superoxide radicals by green fluorescent proteins. *Biochimica et Biophysica Acta 1760*, 1690–1695.

56. Bou-Abdallah, F. and Chasteen, N. D. (2008) Spin concentration measurements of high-spin (g'=4.3) rhombic iron(III) ions in biological samples: theory and application, *J. Biol. Inorg. Chem. 23*, 15-24.

57. Svistunenko, D. A. and Cooper, C. E. (2004) A New Method of Identifying the site of Tyrosyl Radicals in Proteins, *Biophys. J. 87*, 582-595.

58. Zhao, Z., Treffry, A., Quail, M. A., Guest, J. R., and Harrison, P. M. (1997) Catalytic iron(II) oxidation in non-haem ferritin of Escherchia coli; the early intermediate is not an iron tyrosinate, *J. Chem. Soc. Dalton Trans.* 3977-3978.

59. Sun, S. and Chasteen, N. D. (1994) Rapid kinetics of the EPR active species formed during initial iron uptake in horse spleen apoferritin, *Biochemistry 33*, 15095-15102.

60. Grady, J. K., Zang, Jia, Laue, T. M., Arosio, P., and Chasteen, N. D. (2002) Characterization of the H- and L-subunit ratios of ferritins by sodium dodecyl sulfate-capillary gel electrophoresis, *Anal. Biochem. 302*, 263-268.

61. Grady, J. K., Chen, Y., Chasteen, N. D., and Harris, D. C. (1989) Hydroxyl radical production during the oxidative deposition of iron in ferritin, *J. Biol. Chem. 264*, 20224-20229.

Table 1: $Fe(II)/O_2$ ratios calculated from oximetry measurements following the addition of up to 480 Fe(II)/shell added in increments of 48 Fe(II)/shell.[a]

Iron Added (total Fe)	WT EcFtnA	H53A (Site A)	E17A (Site A)	E94A (Site B)	E130A (B&C sites)	E49A (Site C)	E126A (Site C)	Y24F
1st 48 Fe/shell (48)	3.2	3.8	3.8	3.9	2.2	2.2	2.1	2.4
2nd 48 Fe/shell (96)	3.4	3.6	3.4	4.0	3.4	3.2	3.5	2.4
3rd 48 Fe/shell (144)	3.5	3.7	3.9		3.0	3.2	3.3	2.7
4th 48 Fe/shell (192)	3.5				3.0	3.1	3.3	2.9
5th 48 Fe/shell (240)	3.6				3.1	3.3	3.4	3.0
6th 48 Fe/shell (288)	3.7				3.2	3.4	3.5	3.0
7th 48 Fe/shell (336)	3.7				3.2	3.4	3.5	3.2
8th 48 Fe/shell (384)	3.8				3.2	3.7	3.6	3.6
9th 48 Fe/shell (432)	3.9				3.4	3.8	3.7	3.5
10th 48 Fe/shell (480)	3.8				3.3	3.8	3.7	3.6

[a]Table values are from a series of additions to the same protein sample. An average value of $Fe(II)/O_2$ = 3.1 ± 0.2 for the first 48 Fe added to WT EcFtnA was obtained from multiple additions to different protein samples (See text.). Conditions: 1 μM protein in 0.1 M Mops, 50 mM NaCl, pH 7.0

Table 2: Half-lives for Fe(II) oxidation as a function of added Fe(II) calculated from the rate of initial absorbance change at 305nm.[a]

Add. No.	Total Fe Added	WT EcFtnA	H53A (Site A)	E17A (Site A)	E94A (Site B)	E130A (B&C sites)	E49A (Site C)	E126A (Site C)	Y24F	HuHF
1	48	0.115 ± 0.002	650 ± 4	22 ± 1	17.1 ± .5	1.4 ± 0.1	0.110 ± 0.005	1.1 ± 0.3	0.196 ± 0.003	0.0292 ±0.0002
2	96	1.1 ± 0.1	585 ± 1	94 ± 5	280 ± 50	3.8 ±0.5	6.8 ± 0 .1	5.8 ± 0.1	26.3 ± 1.0	5.9 ±0 .2
3	144	7.0 ± 0.6	409 ± 3	69 ± 1		14.4 ± 0.4	7.0 ± 0.2	31.6 ±0.6	29.1 ± .6	7.0 ±0.7
4	192	7.8 ± 0.5	281 ± 3	44 ± 3		17.3 ± 0.7	7.1 ± 0.2	29.5 ± 0.3	28.4 ± 1.0	5.2 ±0.1
5	240	7.2 ± 0.2		42 ± 2		18.9 ± 0.4	6.7 ± 0.2	(10.7 ± 0.1)[b]	30.3 ± .6	6.4 ±0.2
6	288	7.5 ± 0.4				18.1 ± 0.6	7.4 ± 0.2		29.6 ± 1.5	5.2 ±0.1
7	336	7.6 ± 0.4					7.8 ± 0.2			5.5 ±0.2
8	384	6.9 ± 0.6					8.2 ± 0.2			6.0 ±0.4
9	432	7.0 ± 0.6					8.6 ± 0 .2			7.7 ± 0 .5
10	480	8.1 ± 0.5					9.7 ± 0.3			6.8 ± 0.6

[a]Conditions: 1 μM protein in 0.1 M Mops, 50 mM NaCl, pH 7.0. Typical kinetic curves are shown in the absorbance-time curves are indicated. (See Materials and Methods).

[b]Measured one-half hr after 4th addition whereas other measurements were made 2 – 4 min between additions. Note the shorter half-life demonstrating some restored activity.

Table 3: Rate constants from stopped-flow data for the single addition of 48 Fe(II) aerobically to the apoprotein.[a]

Protein	k_1 (s^{-1})	k_2 (s^{-1})	k_2' (s^{-1})
EcFTnA (610 nm)	7.3 ± 0.8	0.136 ± 0.005	0.0214 ± 0.0007
E49A (630 nm)	15.5 ± 2.2	0.83 ± 0.09	0.13 ± 0.01
Y24F (585 nm)	4.1 ± 0.2	0.16 ± 0.01	0.13 ± 0.01
HuHF (650 nm)	31.6 ± 0.7	1.37 ± 0.08	0.244 ± 0.008

[a]Standard errors from curve fitting according to the model $A \xrightarrow{k_1} B \xrightarrow{k_1'} B' \xrightarrow{k_2} C$ are indicated. Conditions: final EcFtnA concentration 1 μM in 0.1 M Mops, 50 mM NaCl, pH 7.0.

FIGURE CAPTIONS

Figure 1: Schematic diagram showing the di-iron nuclear ferroxidase center (A and B) and the third proximal C-site of EcFtnA from *E. coli*. The drawing was made with the ISIS Draw 2.4 program manufactured by MDL (Molecular Design Limited, www.mdl.com) and is based on the Fe(III)-derivative crystal structure of EcFtnA (*10*).

Figure 2: (A) Spectrophotometric and (B) spectrofluorimetric titration curves of EcFtnA with Fe(II) added as 8 Fe(II)/protein/injection for (A) and 10 Fe(II)/shell for (B). Insets: Family of UV-vis and fluorescence titration spectra. (C) Dependence of the initial rate of O_2 consumption and (D) H^+ production on the Fe(II)/protein ratio for multiple sequential additions of 12 Fe(II)/protein. Conditions: 1.0 μM EcFtnA, 0.1 M Mops, 50 mM NaCl, pH 7.0, 25 °C.

Figure 3: Oxygen consumption and proton production curves versus time for four sequential additions of four 12 Fe(II) per EcFtnA. Conditions: 1.12 μM EcFtnA in 0.3 mM Mops, 50 mM NaCl, pH 7.0.

Figure 4: Anaerobic spectrometric titration curves of EcFtnA containing 48 Fe(II)/shell as a function of added hydrogen peroxide under argon atmosphere. *Inset*, family of UV-visible difference spectra. Conditions: 3.5 μM EcFtnA in 0.1 M Mops, 50 mM NaCl, pH 7.0. Each point corresponds to the addition of 0.05 H_2O_2/Fe(II).

Figure 5: (A) X-band EPR signal of the EMPO-OH adduct in the absence or presence of 2 μM protein, 500 μM H_2O_2, 25 mM EMPO, the indicated amount of iron, and 0.1 M Mes, 50 mM NaCl, pH 6.50. The sample volume was 70 μl and all solutions were degassed overnight with pure argon gas. Spectrum a): buffer + EMPO + H_2O_2 + 96 μM Fe(II); spectrum b): EcFtnA in buffer + EMPO + H_2O_2 + 96 μM Fe(II) or 48 Fe(II)/shell; spectrum c): EcFtnA in buffer + EMPO + 96 μM Fe(II) or 72 Fe(II)/shell + H_2O_2; spectrum d): EcFtnA in buffer + EMPO + 96 μM Fe(II) or 48 Fe(II)/shell + H_2O_2; spectrum e): EcFtnA in buffer + EMPO + 72 μM Fe(II) or 36 Fe(II)/shell + H_2O_2. Spectrometer parameters were: microwave power 5.0 mW, modulation amplitude 0.5 G, time constant 163.8 ms, sweep time 83.89 ms, signal averaged four times, room temperature.

Figure 6: (A) Relative initial rate of Fe(II) oxidation and (B) absorbance change as a function of additions of 48 Fe(II) to the protein. Conditions: 1 μM apo-EcFtnA in 0.1 M Mops, 50 mM NaCl, pH 7.0.

Figure 7: Stopped-flow absorbance-time kinetic trace of EcFtnA following aerobic addition of 48 Fe(II) to the apoprotein. The fitted curve and residual as a result of non-linear least squares fitting to the model $A \xrightarrow{k_1} B \xrightarrow{k_2} B' \xrightarrow{k_2'} C$ are indicated. Conditions: final EcFtnA concentration 1 μM in 0.1 M Mops, 50 mM NaCl, pH 7.0.

Figure 8: EPR spectrum of tyrosine radical at 77 K and its decay (inset). 48 Fe(II)/shell was added to apoEcFtnA and the sample frozen after 40 s. Decay curve was generated by thawing and refreezing the sample at various time intervals. Conditions: 11.5 μM EcFtnA in 0.1 M Mops, 50 mM NaCl, pH 7.

Figure 1

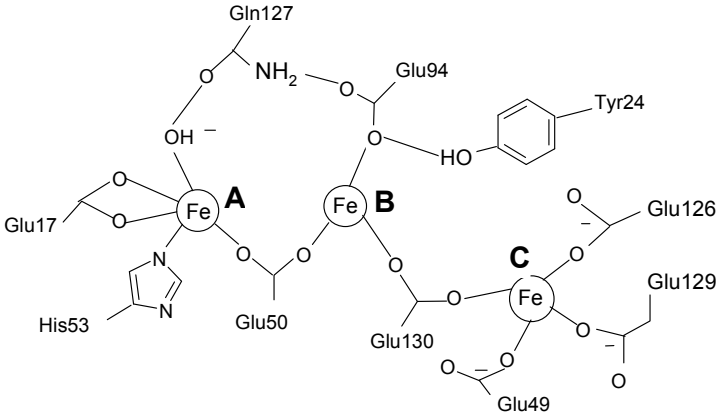

EcFtnA Ferroxidase Center

Figure 2

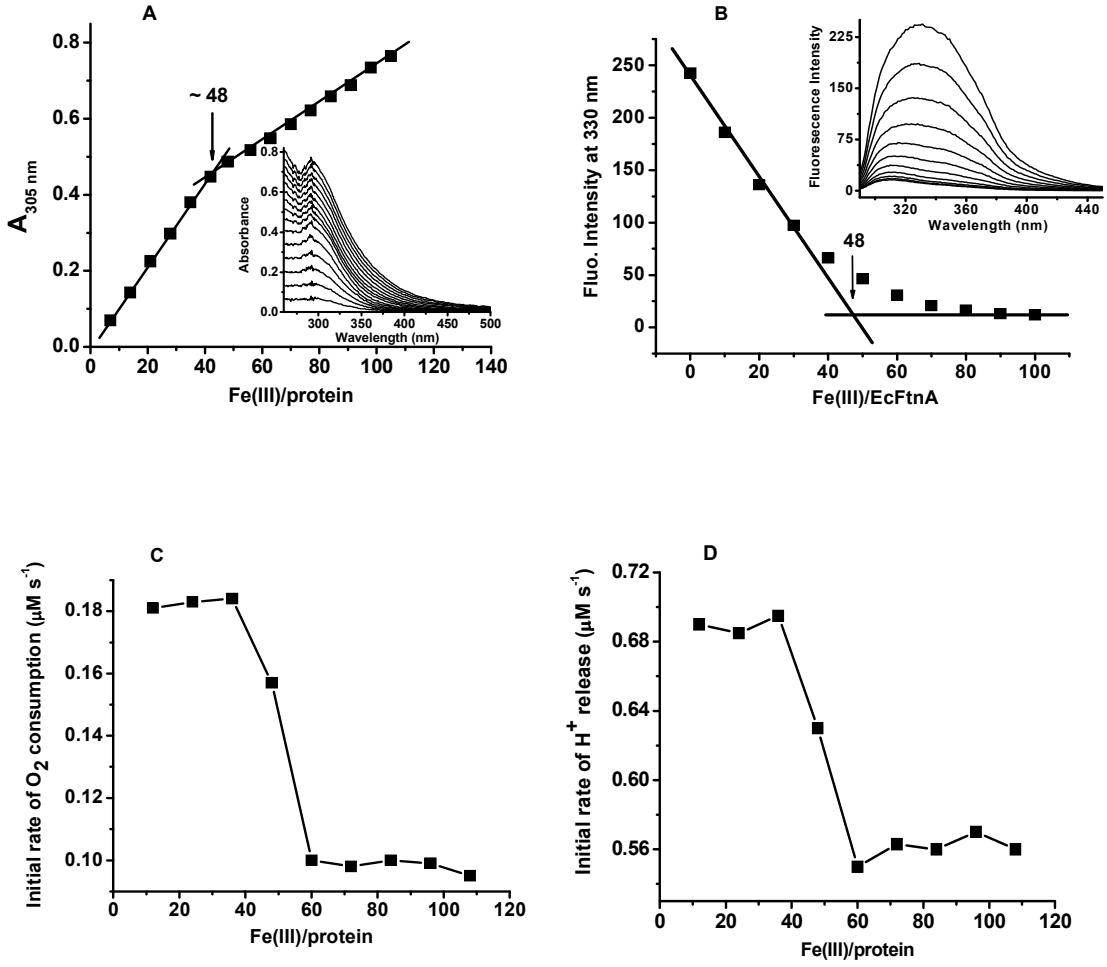

Figure 3

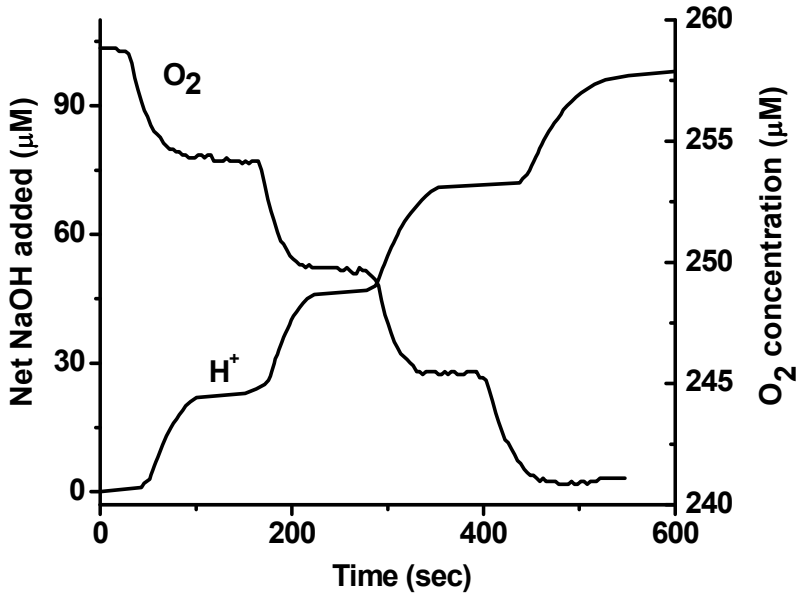

Figure 4

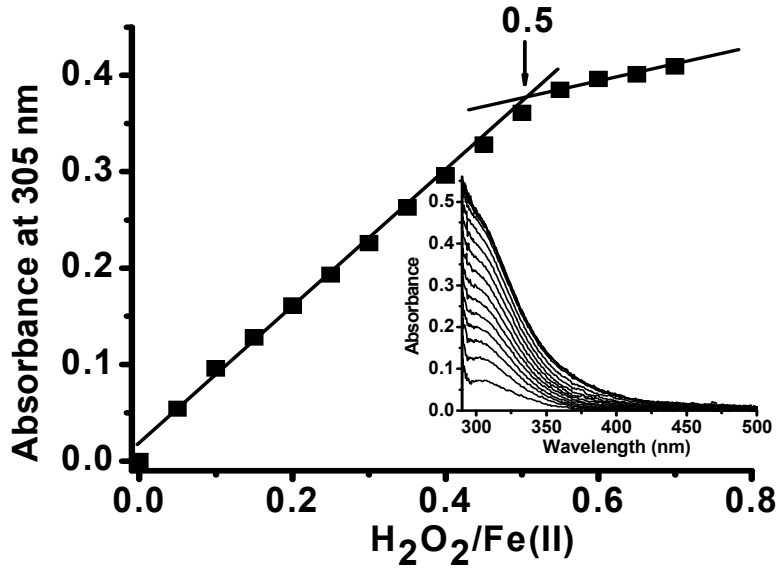

Figure 5

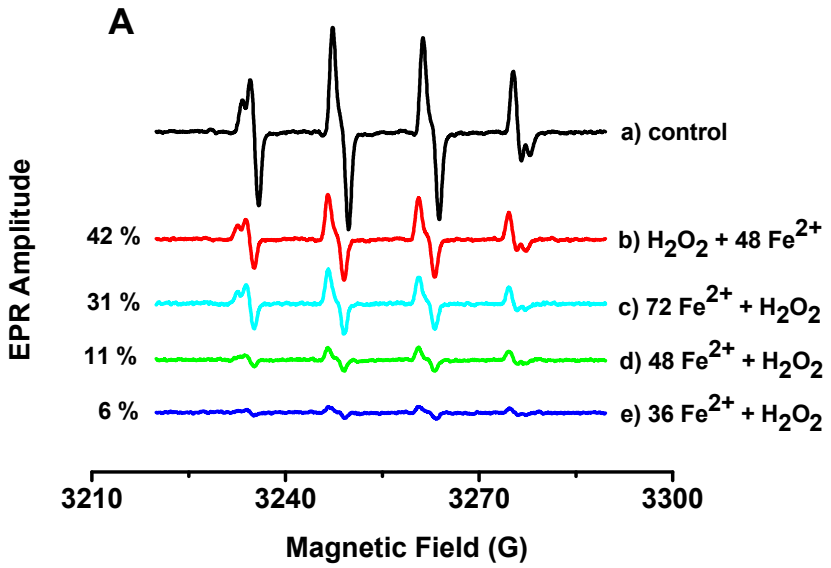

Figure 6

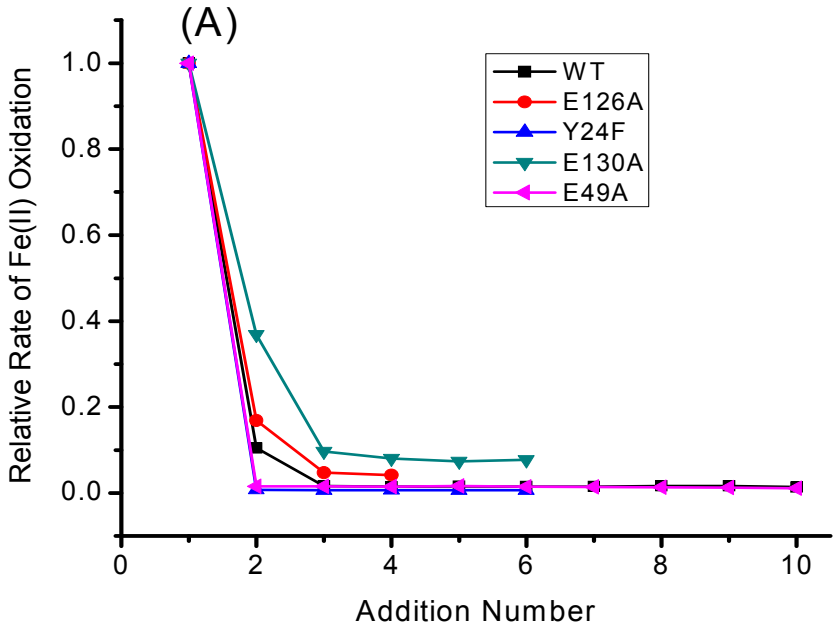

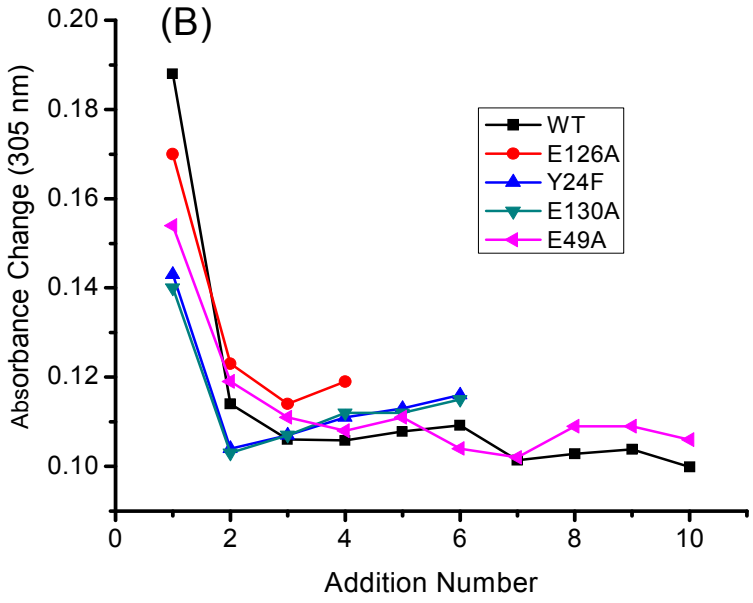
(B)
Absorbance Change (305 nm)
Addition Number
WT
E126A
Y24F
E130A
E49A
0.20
0.18
0.16
0.14
0.12
0.10
0
2
4
6
8
10

Figure 7

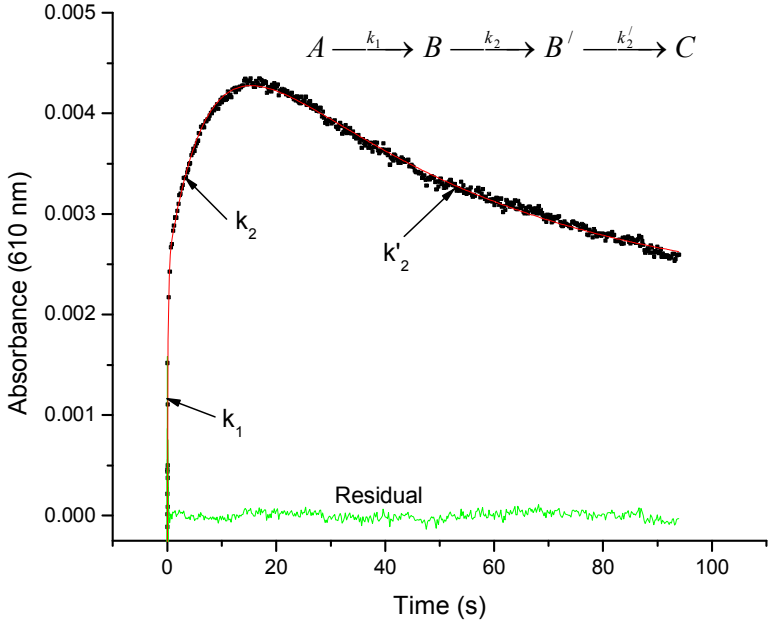
$A \xrightarrow{k_1} B \xrightarrow{k_2} B' \xrightarrow{k_2'} C$
Absorbance (610 nm)
Time (s)
k2
k'2
k1
Residual
0.005
0.004
0.003
0.002
0.001
0.000
0
20
40
60
80
100

Figure 8

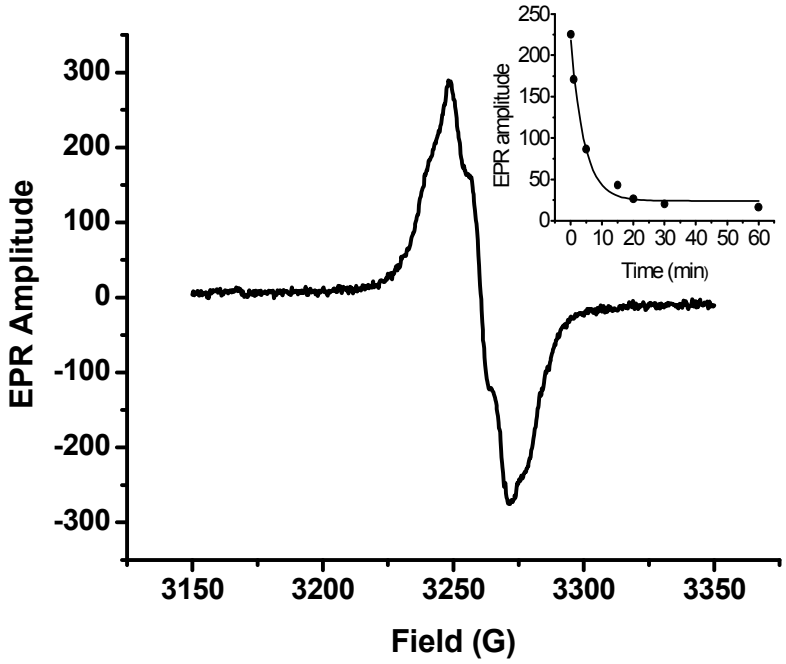
EPR Amplitude
300
200
100
0
-100
-200
-300
3150
3200
3250
3300
3350
Field (G)
EPR amplitude
250
200
150
100
50
0
0 10 20 30 40 50 60
Time (min)